Non-Contact Voltage Monitoring of HVDC Transmission Lines Based on Electromagnetic Fields

Ke Zhu, Wing Kin Lee, and Philip W. T. Pong, *Senior Member, IEEE*

***Abstract*— The high-voltage direct current (HVDC) transmission network is envisioned to advance further as a supplement to AC transmission in a new era of renewable energy and smart grid development. Voltage monitoring of HVDC transmission lines is critical for evaluating the power quality in power delivery and realizing the stability control of the power system. Unfortunately, the traditional potential transformers can only work with AC voltage while the other existing voltage sensors (e.g., Hall-effect voltage sensors, and optical-fiber voltage sensors) are still not practical for large-scale deployment for monitoring the HVDC transmission lines, owing to the fact that they are either invasive or expensive. In this paper, a non-contact electric-coupling-based voltage sensing with the assistance of magnetic-field sensing for monitoring the voltages of HVDC transmission lines is proposed. The voltages of HVDC transmission lines can be reconstructed from measuring the induced voltage of induction bars, and their correlation coefficients are attained by the magnetic sensing with an optimization program which determines their relative spatial positions. The sensitivity and stability of the proposed platform, and the corona effect of the HVDC transmission lines are discussed. The performance of the proposed sensing technique was investigated by simulation on a ±100 kV HVDC transmission line system, and was further experimentally validated on a scaled HVDC transmission-line testbed in the lab. This sensing technique can be implemented at low cost by adopting copper induction bars and magnetoresistive sensors. Considering its non-contact nature and cost-effectiveness, this technique is suitable for a large-scale deployment over HVDC transmission networks for wide-area monitoring.**

***Index Terms*— Voltage, HVDC transmission line, electric coupling, magnetic sensing, magnetoresistive sensor.**

I. Introduction

HIGH-VOLTAGE direct current (HVDC) systems are prevailing because there is a rapidly increasing demand for delivering large quantities of electricity over long distances across different regions [1]–[4]. HVDC transmission networks are being widely recognized and implemented for their advantages such as long-distance bulk-power delivery at a lower capital cost, asynchronous interconnections, and reduced power loss [5], [6]. It is envisioned that the HVDC power transmission will be a critical component of power system in the near future [7], [8].

The voltages of HVDC transmission lines need to be closely monitored for the power quality assessment and system stability control. This is because the DC power is converted from the AC side by rectifiers, which generate harmonics on the HVDC transmission lines. These harmonics can propagate and cause electromagnetic interference both in the power system and in the vicinity of the transmission lines. Therefore, the total harmonic distortion (THD%) of the rectifier output must be below 1.5% for an HVDC transmission network according to the IEEE 519 standards [9]. As such, the voltages of HVDC transmission lines need to be measured for designing the active and passive filters [10] for removing harmonics. Moreover, the voltages of HVDC transmission lines are required to be measured for detecting and identifying short-circuit faults in order to take remedial actions by managing the converters/inverters [4], [11].

The existing voltage sensing technologies are analyzed and summarized in Table I. Their working principles and limitations are compared. They cannot meet the challenge of modern power grids which are continuing to expand and gain in complexity [12]–[14]. Therefore, a new voltage sensor which is galvanically isolated, cost-effective and easy for installation for monitoring HVDC transmission lines is necessary for HVDC development.

In our previous work, a non-contact capacitive-coupling based voltage sensing technique with the assistance of magnetic-field sensing for monitoring voltage of HVAC transmission lines was proposed [15], [16]. In this work, the sensing technique is further extended for HVDC transmission lines specifically. This is feasible because both magnetic sensors and induction bars respond to the static electromagnetic fields. The challenges in this work are (1) how to correlate the voltages of the HVDC transmission lines with the induced voltages of the induction bars mathematically, (2) how to restore the DC signals including specific harmonics effectively from a complex electromagnetic environment (mainly AC) which can also induce the voltage on the induction bars [17]–[19], and (3) how to tackle the corona effect under HVDC transmission lines which is different from the scenario of HVAC transmission lines. In Section II, the voltage relation between HVDC

Manuscript received December 9, 2018; revised January 9, 2019; accepted January 9, 2019. Date of publication January 11, 2019; date of current version March 18, 2019. This work was supported in part by the Seed Funding Program for Basic Research, in part by the Seed Funding Program for Applied Research and Small Project Funding Program from the University of Hong Kong, in part by the ITF Tier 3 Funding under Grant ITS-104/13 and Grant ITS-214/14, in part by the RGC General Research Fund under Grant 17204617, and in part by the University Grants Committee of Hong Kong under Grant AoE/P-04/08. The associate editor coordinating the review of this paper and approving it for publication was Dr. Jürgen Kosel. *(Corresponding author: Philip W. T. Pong.)*

The authors are with the Department of Electrical and Electronic Engineering, The University of Hong Kong, Hong Kong (e-mail: zhuke@connect.hku.hk; wklee@eee.hku.hk; ppong@eee.hku.hk).

Digital Object Identifier 10.1109/JSEN.2019.2892498

TABLE I
COMPARISON OF EXISTING VOLTAGE SENSORS

Sensor	Meas.	Principle	Limitations
Potential transformer [20]	AC	Electromagnetic induction	(1) Invasive: high voltage hazard, difficult for installation; (2) High cost: insulation design; (3) Limited measurement: not work for DC network;
Hall voltage sensor [21]	AC+DC	Hall Effect and magnetic compensation principle	(1) Invasive: high voltage hazard, difficult for installation; (2) High cost: the usage of high voltage resistance and insulation design;
Optical fiber voltage sensor [22-25]	AC+DC	Pockels effect	High cost: light transmitters and optical components are needed;
AC voltage probe [26]	AC	Capacitive-coupled current cancellation	(1) High cost: a voltage generator inside for generating the balanced current; (2) Limited measurement: not work for DC network;
Capacitively coupled voltage sensor [27]	AC+DC	Capacitive divider	Limited measurement: only applicable for single-phase conductor;

transmission lines and induction bars are established, and the process for monitoring the voltages of HVDC transmission lines by the proposed sensing technique are introduced. The sensing sensitivity under various layouts are displayed. The stability and corona effects are also discussed. The feasibility of the sensing technique is demonstrated on a ± 100 kV HVDC transmission lines by simulation as discussed in Section III. The technique was also experimentally validated by a scaled HVDC transmission-line testbed in the lab. The details are explained in Section IV. Conclusion and future work are included in Section V.

II. METHODOLOGY

The voltages induced on the induction bars by the voltages in the HVDC transmission lines through electric coupling can be measured. The spatial distances between the HVDC transmission lines and the induction bars can be determined by sensing the magnetic fields emanated from the currents in the HVDC transmission lines with an optimization algorithm. The details of correlating the voltages between HVDC transmission lines and induction bars, and the flowchart of the sensing technique are elaborated as follows.

A. Voltage Correlation

The electric coupling describes the energy coupled between one object and another through electric field. Since the energy transfer is through electro-magnetic induction rather than electromagnetic wave, the coupling between objects can be represented by a lumped capacitor. The equivalent capacitors among HVDC transmission lines, induction bars and the ground are shown in Fig. 1(a). The capacitance (C_{i0} is the self-capacitance between a conductor and the ground, C_{ij} is the mutual-capacitance between conductors) in the network can be attained by

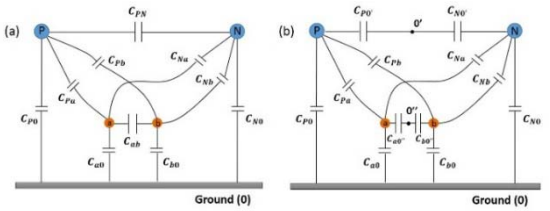

Fig. 1. Capacitors formed among HVDC transmission lines, induction bars and ground. (a) Electric circuit formed by capacitors. (b) Equivalent electric circuit by transforming the null potential for the transmission lines and induction bars.

$$C_{i0} = \beta_{iP} + \beta_{iN} + \beta_{ia} + \beta_{ib} \quad (i = P, N, a, b) \tag{1}$$

$$C_{ij} = -\beta_{ij} \quad (i = P, N, a, b, j = P, N, a, b, i \neq j) \tag{2}$$

$$\begin{pmatrix} Q_P(t) \\ Q_N(t) \\ Q_a(t) \\ Q_b(t) \end{pmatrix} = \begin{pmatrix} \beta_{PP} & \beta_{PN} & \beta_{Pa} & \beta_{Pb} \\ \beta_{NP} & \beta_{NN} & \beta_{Na} & \beta_{Na} \\ \beta_{aP} & \beta_{aN} & \beta_{aa} & \beta_{ab} \\ \beta_{bP} & \beta_{bN} & \beta_{ba} & \beta_{bb} \end{pmatrix} \begin{pmatrix} V_P(t) \\ V_N(t) \\ V_a(t) \\ V_b(t) \end{pmatrix} \tag{3}$$

in which $V_i (i = P, N, a, b)$ is the potential of each conductor, $Q_i (i = P, N, a, b)$ is the electrical charge of each conductor, and $\beta_{ij} (i, j = P, N, a, b, i \neq j)$ is the inductive potential coefficients which depends on the relative spatial positions between conductors [16]. After transforming the null potential points for transmission lines ($0'$) and induction bars ($0''$) in [28, Fig. 1(b)], their potentials are the same as the ground which can be represented by the electric circuit in Fig. 2(a). By expressing the capacitors in impedances (Fig. 2(b)), the voltages of the HVDC transmission lines (V_P and V_N) and the induction bars (V_a and V_b) can be correlated as

$$\begin{bmatrix} V_a \\ V_b \end{bmatrix} = \begin{bmatrix} \dfrac{Z_a Z_{pab}}{(Z_{pa}+Z_a)(Z_{pab}+Z_p)} & \dfrac{Z_a Z_{Nab}}{(Z_{Na}+Z_a)(Z_{Nab}+Z_N)} \\ \dfrac{Z_b Z_{pab}}{(Z_{pb}+Z_b)(Z_{pab}+Z_p)} & \dfrac{Z_b Z_{Nab}}{(Z_{Nb}+Z_b)(Z_{Nab}+Z_N)} \end{bmatrix} \times \begin{bmatrix} V_P \\ V_N \end{bmatrix} \tag{4}$$

where

$$Z_{Pab} = \frac{(Z_{pa} + Z_a)(Z_{pb} + Z_b)}{(Z_{pa} + Z_a) + (Z_{pb} + Z_b)} \tag{5}$$

$$Z_{Nab} = \frac{(Z_{Na} + Z_a)(Z_{Nb} + Z_b)}{(Z_{Na} + Z_a) + (Z_{Nb} + Z_b)} \tag{6}$$

Therefore, the voltages of the HVDC transmission lines can be monitored via the simultaneous voltage measurement of the induction bars based on Eq. (4).

B. Voltage Reconstruction

The structure of this voltage-sensing platform was developed as displayed in Fig. 3. The induction bars are located on the ground level with the magnetic sensors above them (Fig. 3(a)). Since the orientation of HVDC transmission

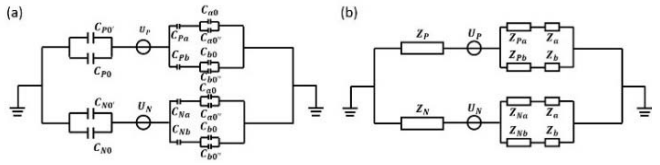

Fig. 2. Electric circuit for coupling voltage of HVDC transmission lines and induction bars. (a) Circuit denoted by capacitors. (b) Circuit formed by equivalent impedance.

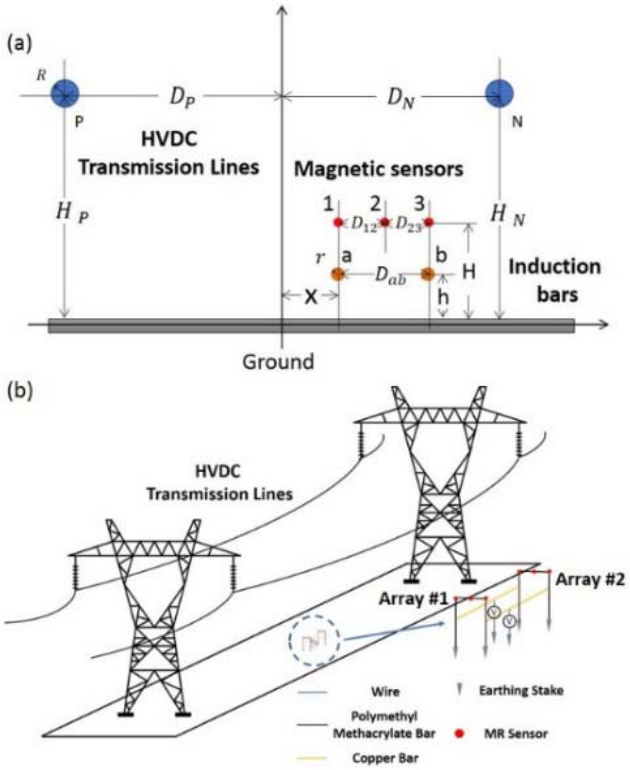

Fig. 3. Layout of HVDC transmission lines, induction bars and magnetic sensors. (a) The altitude of pole P and N, induction bars, and magnetic sensors are H_P, H_N, h and H, respectively. The spatial distance between the pole P (N) and the central line is $D_p(D_n)$. The spatial distance between magnetic sensors (induction bars) are D_{12} and D_{23} (D_{ab}). The horizontal displacement between induction bar a and the central line is x. (b) 3D graph of HVDC transmission lines and voltage-sensing platform.

lines at each span may not be definitely available from the power company, two arrays (array #1 and #2 in Fig. 3(b)) of magnetic sensors are deployed to determine the spatial positions and orientation of transmission lines so that the direction of induction bars can be aligned with the HVDC transmission lines. The flowchart of this technique to monitor the voltages of the HVDC transmission lines [15], [16] is shown in Fig. 4. Firstly, the magnetic-field signals (B_m) and induced voltages (V_m) are measured respectively. These signals are filtered to remove the electromagnetic interferences from the background while retaining the components generated from the HVDC transmission lines. Secondly, the spatial positions of the HVDC transmission lines (P) are reconstructed from the filtered magnetic-field signals (B_m') in the source position optimization (SPO). The details of SPO can be found in [15], [16], and [29]. With the filtered induced voltage (V_m') and attained positions of the HVDC transmission lines (P),

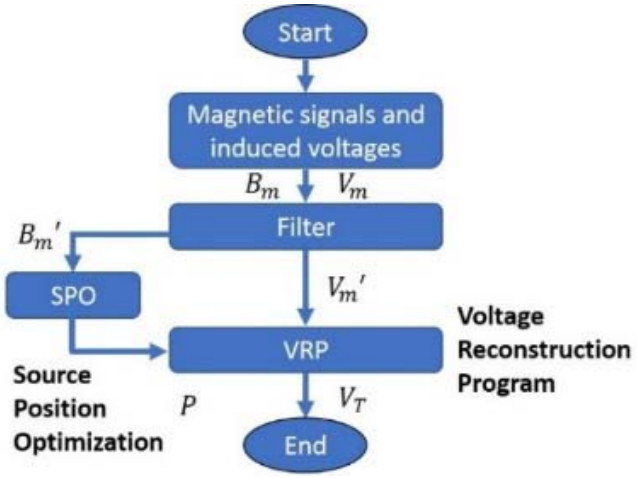

Fig. 4. Flowchart of the voltage-sensing technique to monitor the voltages of HVDC transmission lines [15], [16].

the voltages of the HVDC transmission lines (V_T) can be determined in the voltage reconstruction program (VRP) based on [15, eq. (4)], [16], and [29].

C. Voltage-Sensing Sensitivity

The voltage-sensing sensitivity is defined as the ratio of the induced voltage of an induction bar to the voltage of the corresponding HVDC transmission line:

$$S_a = \frac{U_a}{U_P} \tag{7}$$

$$S_b = \frac{U_b}{U_N} \tag{8}$$

where U_a, U_b are the induced voltages on the induction bars a and b respectively, U_P, U_N are the voltages of HVDC transmission lines P and N respectively, and S_a, S_b are the sensitivities of the induction bar a and b, respectively. The induced voltages and thus the voltage-sensing sensitivities vary under different layouts of HVDC transmission lines and induction bars because the electric fields are not evenly distributed in the space. The dependences of the voltage-sensing sensitivities (S_a, S_b) on horizontal position (x), spacing distance between induction bars (D_{ab}), and height (h) (Fig. 5(a)) were studied. From Fig. 5(b), it can be seen that the largest sensitivity can be achieved when the induction bar is directly below the transmission line. This is because the resultant electric field is strongest under a transmission line where the canceling effect from the other one (opposite polarity) is weakened. The study on sensitivity of different spacing distances and heights were conducted by fixing the position of bar a (under the negative transmission line for achieving the largest sensitivity as indicated in Fig. 5(b)) while increasing the spacing distance between induction bars and their height. The result (Fig. 5(c)) shows that the sensitivity of induction bar a increased slightly between 0 to 4 m (the increased sensitivity of induction bar b in this range was mainly caused by the change of its horizontal displacement), while remained almost unchanged afterwards. This revealed that the a larger spacing distance can contribute the increase of sensitivity but

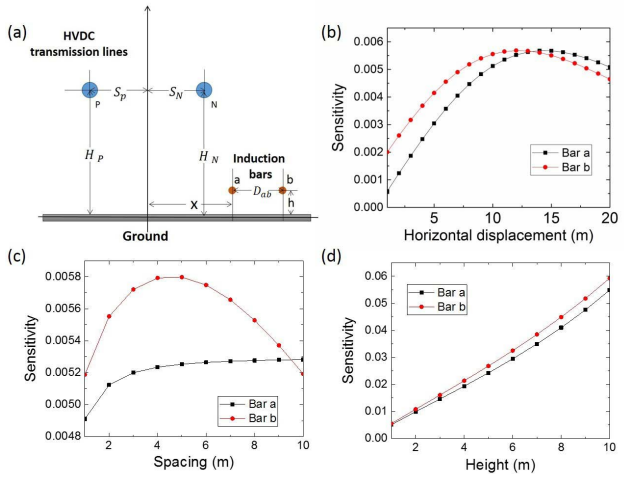

Fig. 5. Voltage-sensing sensitivity study under various layouts of HVDC transmission lines and induction bars. (a) Layout of HVDC transmission lines: spacing distance $D_P = D_N = 10\ m$, height $H_P = H_N = 20\ m$, and length 100 m. Layout of induction bars: length 1 m. (b) Layout of induction bars: spacing distance $D_{ab} = 2$ m, height $h = 1$ m, and horizontal displacement $x = 1, 2, 3 \ldots 20$ m. (c) Layout of induction bars: horizontal displacement $x = 10$ m, height $h = 1$ m and spacing distance $D_{ab} = 1, 2, 3 \ldots 10$ m. (d) Layout of induction bars: horizontal displacement $x = 10$ m, spacing distance $S_{ab} = 2$ m, and height $h = 1, 2, 3 \ldots 10$ m.

its effect is limited [16]. The sensing sensitivities were also enhanced with a higher position of induction bars (Fig. 5(d)). However, the size and height of the sensing platform are preferred to be compact in practice for easier installation. Therefore, the optimum choice for achieving a high sensitivity of the developed sensing platform is to place them directly below a transmission line at near ground level.

D. Corona Effect

Though the high-voltage transmission lines are suitable for long-distance power transmission, the corona effect is exhibited when the voltage (i.e., electric field) of the transmission conductor is strong enough [30], [31]. The ionic space charges are generated in the vicinity of a conductor when corona discharge occurs. For HVAC transmission lines, the ions generated in the first half cycle are almost pulled back to the wire due to the change in voltage polarity in the second half cycle. As such, there is nearly charged ions in the space between the pole wires and ground [32]. However, for HVDC transmission lines, the ions migrate to the surrounding and the ground under the action of the electric field force because their pole polarity is fixed. In the presence of ions, the ground-level electric field can be strengthened [33]. This electric field, caused by the interaction of the space charge and the original wire charge, is called a combined electric field. The distribution of ion flow field and electric field strength of a bipolar HVDC transmission lines are depicted in Fig. 6. The entire space can be divided into three areas as shown in Fig. 6(a): (1) region with the positive ions between the positive pole and the ground, (2) region with the negative ions between the negative pole and the ground, and (3) region with the coexisting positive and negative ions between the positive and negative poles [33], [34]. The electric fields with and without considering the corona effect are depicted in Fig. 6(b).The

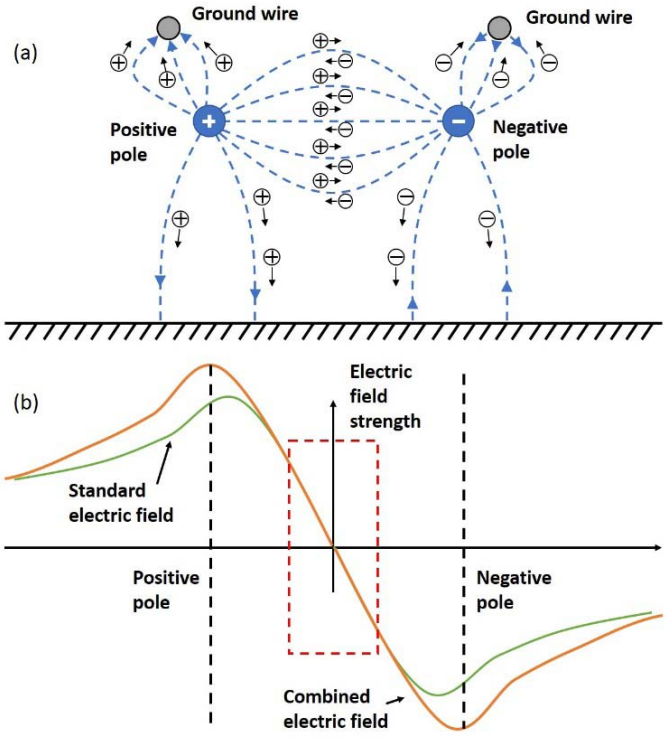

Fig. 6. Corona effect under a bipolar HVDC transmission line. (a) Distribution of ion flow field includes the positive ions between the positive pole and the ground, the negative ions between the negative pole and the ground, and the coexisting positive and negative ions between the positive and negative poles. (b) Electric field strength under a bipolar HVDC transmission line with and without considering the corona effect.

electric fields are with the minimal distortion around the central positions because the influences from the positive and negative ions of corona effects are neutralized [35], [36]. The voltages of the induction bars are purely induced from the electric fields generated from the HVDC transmission lines. Therefore, it is recommended that the induction bars should be located in the vicinity of the central location of HVDC transmission lines to avoid the influence of the corona effect though the sensitivity is strongest under a HVDC transmission conductor as disclosed in Section II(C). It is worth mentioning that research efforts are being made to minimize the corona effects such as by increasing the conductor size and conductor spacing [37], [38]. These efforts are conducive to applying the developed sensing technique under the HVDC transmission lines.

E. Induced Voltage Measurement

For the sake of an accurate measurement for the induced voltage of induction bars, there are some issues to be addressed:

(a) Location of induction bars: there are ion flow fields distributed in the space of HVDC transmission lines as indicated in Section II(D). If the isolated conduction is attached with these charges, a certain potential will be generated. As such, the induction bars should be located in the vicinity of the central location of HVDC transmission lines as disclosed in Section II(D). This is because

that both the positive and negative ions inject into the induction bars simultaneously in this area (as shown in Fig. 6(a)). They are neutralized and do not induce the extra voltage.

(b) Resistance of measurement probe: the resistance of the measurement probe must be high enough (e.g., above hundreds MΩ [39]) to prevent the induced charges of the induction bars from flowing into the ground; otherwise, the induced voltage can be affected.

The stability of this method also depends on the electrical potential of the earthing stake. Typically, the electrical potential is connected to the earth and its electrical potential should be zero [40]. In the normal operating status, the proposed platform should be stable. However, there can be an earth potential rise when the current flows into the earth (e.g., phase-to-ground short-circuit fault). The potential is highest at the point where the current enters the ground, and declines with distance from the source. For the overhead transmission lines, the faulty currents generally flow into the ground through the grounding electrodes at the transmission towers [41], [42]. As such, the platform is recommended to locate at the middle of towers to stay away from the towers to minimize the instability.

F. Other Effects

The effects of ground wires, measurement instrument, and transient response bandwidth are the same as in the study for the HVAC transmission lines: (a) the ground wires in induced voltage analysis are ignored since they would not affect the electric field distribution under HVDC transmission lines; (2) the capacitance of measurement instrument should be considered; and (3) the frequency bandwidth for the voltage-sensing platform is up to MHz. More details can be found in [16].

III. Simulation Validation

In the simulation, a ±100 kV HVDC transmission line interconnecting two identical AC systems (230 kV, 2000 MVA, 50 Hz) was modeled in [6, Fig. 7]. The height of HVDC transmission lines (induction bars) was 20 m (1 m), and the spacing distance of transmission lines (induction bars) was 20 m (2 m). The height of magnetic sensors (H in Fig. 3(a)) was 1.5 m, which was 0.5 m higher than the induction bars (the magnetic sensors were installed at both ends of induction bars as shown in Fig. 3(b)). The horizontal displacement of induction bar *a* (x in Fig. 3(a)) was 1 m. The length of the induction bar was 1 m. The system was initiated and became steady at 0.5 s after a transient duration.

The simulation was conducted under normal operation of HVDC system and under faulted condition, respectively. The three-phase short-circuit fault was simulated at 1.5 s. The sampling rate of the sensor was set as 20 kHz. The transmitted DC power was almost halted during the three-phase fault. The DC voltage increased to 1.2 p.u. because the DC side capacitance was being excessively charged. The function of DC voltage control overrode in the active power control in Station 1 and limited the DC voltage within a

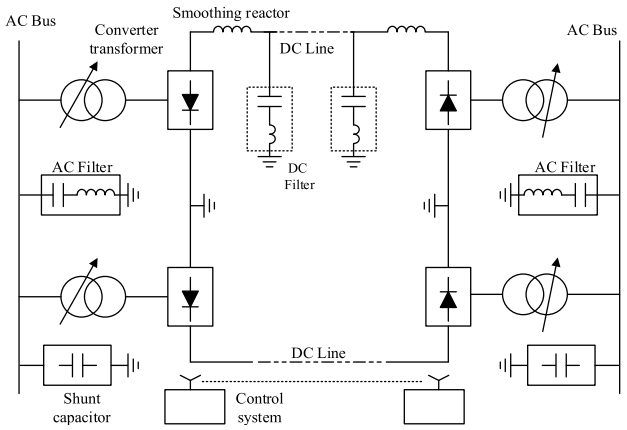

Fig. 7. Geometric configuration of a bi-polar HVDC transmission system.

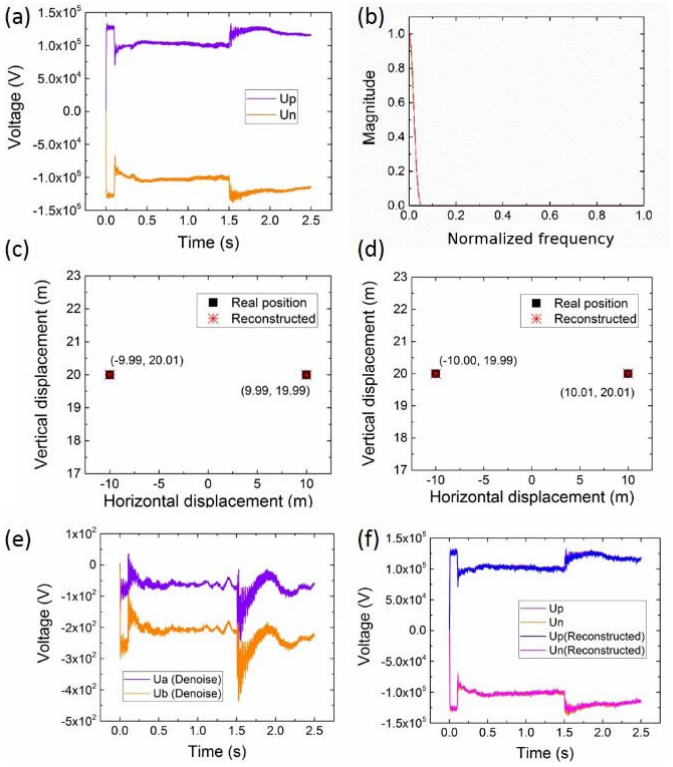

Fig. 8. HVDC transmission-line voltage reconstruction from the induced voltages of the induction bars. (a) Voltage of HVDC transmission lines for a three-phase short-circuit fault at the 1.5 s. (b) Normalized frequency response for a low-pass filter. (c) Position reconstructed from magnetic fields measured by the array #1 of magnetic sensors. (d) Position reconstructed from magnetic fields measured by the array #2 of magnetic sensors. (e) Voltages measured on the induction bars after de-noising. (f) Comparison of HVDC transmission-line voltages and the reconstructed voltages.

fixed range, resulting in the excessive voltage being reduced gradually (Fig. 8(a)). As mentioned in Section II (B), a low-pass filter was designed to remove the high-frequency background noises (kHz ∼ MHz). The normalized frequency response (a ratio of frequency to the reciprocal of sampling rate) of the low-pass filter is shown in Fig. 8(b). In this case, a 30 dB signal-to-noise ratio (SNR) was simulated for the strength of the background noise according to [43] where the noise was measured at power transmission areas. The respective reconstructed position by the two magnetic sensor arrays for the HVDC transmission lines are depicted

in Fig. 8 (c) and (d), where the reconstructed positions matched with the actual ones. The voltages measured on the induction bars after de-noising are shown in Fig. 8(e). Based on the reconstructed positions and the measured induced voltages, the voltages of HVDC transmission lines were restored in Fig. 8(f) which matched with the actual voltages very well. The result shows that the voltages of HVDC transmission lines could be successfully reconstructed from the induced voltages on the induction bars, verifying the feasibility of the proposed sensing technique.

IV. Experiment and Discussion

The experiment was conducted in the lab to verify the practicality of the proposed technique. The schematic drawing of the sensing platform comprised of induction bars and magnetic sensors under the scaled HVDC transmission lines is displayed in Fig. 9 (a). The magnetoresistive (MR) sensors are deployed for this technique because of their advantages:

(1) High sensitivity: MR sensors are much more sensitive than other magnetic solid-state effects, such as the Hall effect (e.g., Hall effect sensor: ∼0.05 mV/V/Oe, anisotropic MR sensor: ∼1 mV/V/Oe, giant MR sensor: ∼3 mV/V/Oe, and tunnel MR sensor: ∼100 mV/V/Oe [44]). MR sensors can measure weak magnetic fields very accurately.

(2) Large frequency bandwidth: MR sensors have a large bandwidth from DC to MHz [14], [45], [46]. They are able to measure the high-frequency transient signals such as harmonics in HVDC transmission lines.

(3) Low power consumption: MR sensors can be specially designed with high internal resistance to reduce their working current (e.g., Hall effect sensor: 5∼20 mA, anisotropic MR sensor: 1∼10 mA, giant MR sensor: 1∼10 mA, and tunnel MR sensor: 0.001∼0.01 mA [44]). As such, they are well suited for the field measurement powered by battery.

(4) Strong durability: MR sensors are invulnerable to extreme temperatures (e.g. operating between −40°C to 120°C, and 30 mins survival at 250°C), dirt or solar radiation [14]. This enable them to work under HVDC transmission lines where the sensors are exposed to outdoor environment.

(5) Easy installation: MR sensors are inherently compact (several mm^2 [44]) and they measure the magnetic field emanated from the conductor non-contactly with no insulation concern. They can be easily installed under the HVDC transmission lines and occupy minimal corridor space.

The compact-in-size (19×25.4 mm^2) magnetoresistive sensors (HMC2003, Honeywell [47]–[49]) were deployed. The copper induction bars were used. The aluminum board was paved as the virtual ground and was connected to the building ground. The HVDC transmission lines were energized by a programmable DC + AC power source (Model 61704, Chroma) with 700 W resistive loadings, and the programmed voltage waveforms measured by the oscilloscope (DPO 2024B, Tektronix) are shown in Fig. 10(a). The HVDC transmission lines were operated in the steady states after the system was energized. The DC offset voltage was 150 V with 600 Hz harmonics (ripple frequency was $6k$ where k was 12 representing a 12-pulse converter in the case [50]). Then the system was programmed to encounter a three-phase short-circuit fault at AC side (same as the condition in simulation part), resulting in a sudden voltage rise afterwards.

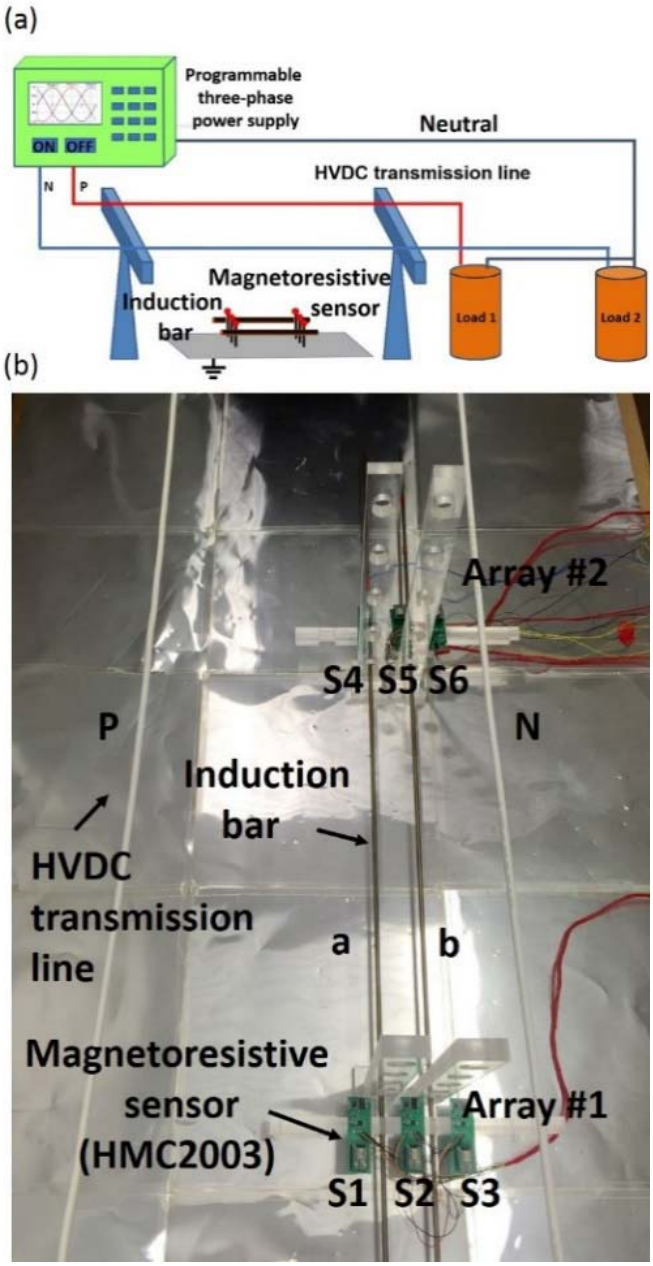

Fig. 9. Experimental setup with the scaled HVDC transmission-line testbed and voltage-sensing platform. (a) Schematic drawing for the testbed consisting of HVDC transmission lines, induction bars and magnetoresistive sensors. (b) Photo of the HVDC transmission-line testbed and the voltage sensing platform. Altitude of HVDC transmission lines (induction bars) is 0.5 m (0.04 m), spacing distance of HVDC transmission lines (induction bars) is 0.16 m (0.06 m), radius of HVDC transmission lines (induction bars) is 0.001382 m (0.003 m), spacing distance of magnetoresistive sensors is 0.06 m, the altitude of magnetoresistive sensor is 0.06 m, and the horizontal displacement (x in Fig. 3) is 0.08 m. The magnetoresistive sensors are numbered S1, S2, S3 for the Array #1, and S4, S5, S6 for Array #2, respectively.

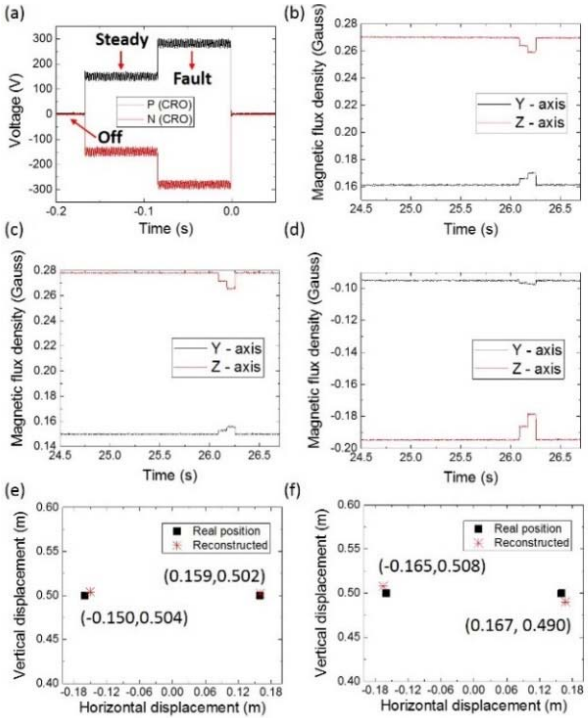

Fig. 10. Voltages measured on HVDC transmission lines, magnetic fields measured by magnetoresistive sensors, and spatial position reconstruction of HVDC transmission lines. (a) Voltages in steady states: positive pole (P): $U_p = 150 + 10sin(12\omega t)$, and negative pole (N): $U_p = -150 + 10sin(12\omega t)$. (b) Magnetic signals from sensor S1 over time. (c) Magnetic signals from sensor S2 over time. (d) Magnetic signals from sensor S3 over time. (e) Spatial position of HVDC transmission lines reconstructed from the data of Array #1. (f) Spatial position of HVDC transmission lines reconstructed from the data of Array #2.

The magnetic fields were measured by the two arrays of magnetoresistive sensors. The magnetic signals measured by the Array #1 (sensors S1, S2 and S3) are shown in Fig. 10 (b), (c) and (d) as an example, respectively (the signals measured by sensors S4, S5 and S6 are similar). The mean values of the magnetic fields in the steady states were input to the stochastic optimization algorithm, and the spatial positions of HVDC transmission lines were reconstructed with the algorithm involving stochastic optimization algorithm as stated in Fig. 4. The real and reconstructed spatial positions of HVDC transmission lines (P and N) based on the measurement of two arrays are displayed in Fig. 10(e) and (f). The directions of the induction bars were then aligned with the HVDC transmission lines based on the reconstructed spatial position of HVDC transmission lines which are very close to the real positions. These reconstructed positions were also used to derive the coefficients correlating the voltage between HVDC transmission lines and induction bars using Eq. (4) – (6).

The induced voltages of the induction bars after removing the background 50 Hz signals due to other mains power supply in the labs [51] are plotted in Fig. 11(a) and (b). Since the voltage sensing platform was exposed to a world of electromagnetics (e.g., electronic devices, radio waves and Wi-Fi) [52], [53], induced voltages due to these random noises existed on the induction bars. These random noises need to be minimized; otherwise they would be amplified in the voltage reconstruction of HVDC transmission lines. The

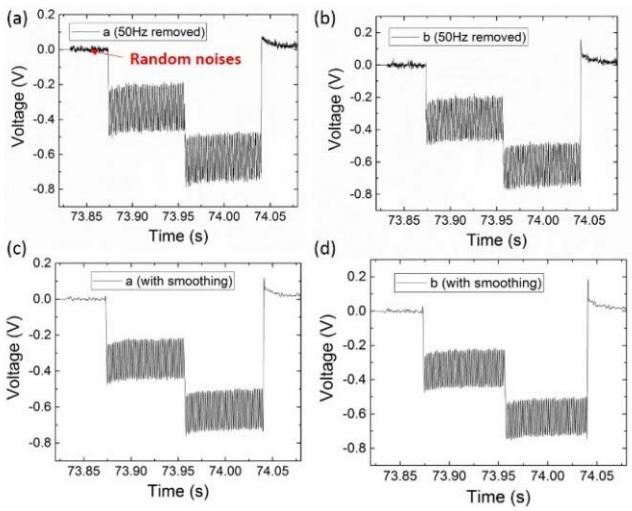

Fig. 11. Voltage measured from the induction bars. (a) Induced voltage of induction bar *a* after removing the 50 Hz signals. (b) Induced voltage of induction bar *b* after removing the 50 Hz signals. (c) Induced voltage of induction bar *a* after removing random noises by smoothing. (d) Induced voltage of induction bar *b* after removing random noises by smoothing.

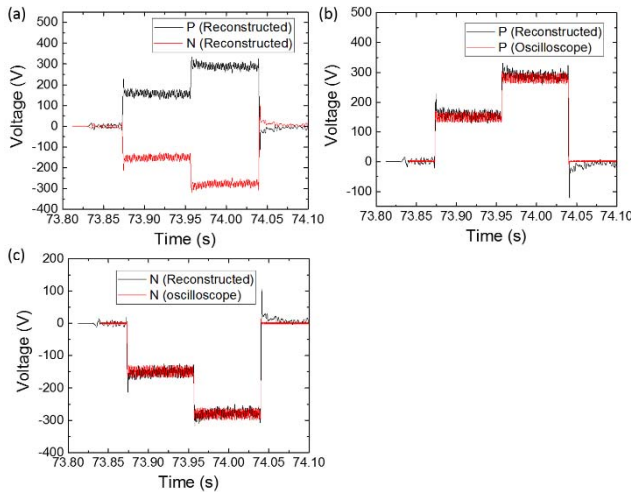

Fig. 12. Reconstructed voltages of HVDC transmission lines. (a) Reconstructed voltage for HVDC transmission lines P and N. (b) Comparison between the reconstructed voltage and the measured voltage of HVDC transmission line P by the oscilloscope. (c) Comparison between the reconstructed voltage and the measured voltage of HVDC transmission line N by the oscilloscope.

Savitzky-Golay filter (25 points of window) which excels in handling the random noises [54] was used as the smoothing method. The induced voltage after the processing is shown in Fig. 11 (c) and (d), and they were input to reconstruct the voltage of HVDC transmission lines. The reconstructed voltage of HVDC transmission lines are displayed in Fig. 12 (a). The reconstructed voltage and the voltage measured by the oscilloscope on the HVDC transmission lines P and N are shown in Fig. 12 (b) and (c) respectively, and it can be seen that the reconstructed voltages are consistent with the voltages of the HVDC transmission lines measured by the oscilloscope.

V. Conclusion and Future Work

In this paper, a non-contact voltage-sensing technique for monitoring the voltages of HVDC transmission lines is proposed. The non-contact measurement is based on the electric

coupling between the HVDC transmission lines and the induction bars. The correlation coefficients between the HVDC transmission lines and the induction bars are dependent on the spatial distances which can be determined by the magnetic-field sensing with an optimization algorithm. Various layouts of induction bars (e.g., horizontal displacement, spacing distance and height) were studied, and it was found that largest sensitivity can be achieved by placing the induction bars directly below the corresponding HVDC transmission lines. The corona effect of HVDC transmission lines and stability of the sensor were also discussed. The performance of the proposed sensing technique was evaluated on a ± 100 kV HVDC transmission line system by simulation, and was also experimentally tested and validated on a scaled HVDC transmission-line testbed in the lab. This sensing technique can be implemented at low-cost by deploying magnetoresistive sensors and copper induction bars. The developed technique has the unique advantage of being non-contact to the HVDC transmission lines which is very important for the safety of serviceman and for the convenience of installation. The advancement on galvanic isolation and low cost is conducive to their large-scale deployment over HVDC transmission networks for wide-area measurement [55], [56].

Future work will focus on validating the developed sensing technique on-site with the real corona effect under a bipolar HVDC transmission line in the field. This will help putting this technique into real application in industry.

REFERENCES

[1] J. W. Feltes, B. D. Gemmell, and D. Retzmann, "From smart grid to super grid: Solutions with HVDC and FACTS for grid access of renewable energy sources," in *Proc. IEEE Power Energy Soc. General Meeting*, Jul. 2011, pp. 1–6.

[2] N. M. Kirby, L. Xu, M. Luckett, and W. Siepmann, "HVDC transmission for large offshore wind farms," *Power Eng. J.*, vol. 16, pp. 135–141, Jun. 2001.

[3] G. Tang, X. Luo, and X. Wei, "Multi-terminal HVDC and DC-grid technology," *Proc. Chin. Soc. Elect. Eng.*, vol. 33, pp. 8–17, Apr. 2013.

[4] M. Singh, V. Khadkikar, A. Chandra, and R. K. Varma, "Grid interconnection of renewable energy sources at the distribution level with power-quality improvement features," *IEEE Trans. Power Del.*, vol. 26, no. 1, pp. 307–315, Jan. 2011.

[5] M. P. Bahrman and B. K. Johnson, "The ABCs of HVDC transmission technologies," *IEEE Power Energy Mag.*, vol. 5, no. 2, pp. 32–44, Mar./Apr. 2007.

[6] M. Szechtman, T. Wess, and C. V. Thio, "A benchmark model for HVDC system studies," in *Proc. Int. Conf. AC DC Power Transmiss.*, Sep. 1991, pp. 374–378.

[7] C. Cecati, G. Mokryani, A. Piccolo, and P. Siano, "An overview on the smart grid concept," in *Proc. 36th Annu. Conf. IEEE Ind. Electron. Soc.*, Nov. 2010, pp. 3322–3327.

[8] K. Zhu, W. K. Lee, and P. W. T. Pong, "Fault-line identification of HVDC transmission lines by frequency-spectrum correlation based on capacitive coupling and magnetic field sensing," *IEEE Trans. Magn.*, vol. 54, no. 11, Nov. 2018, Art. no. 4001805.

[9] (2003). *Interpreting IEEE STD 519 and Meeting its Harmonic Limits in VFD Applications*. Accessed: Apr. 13, 2017. [Online]. Available: http://ow.ly/KnpU30aOY28

[10] W. Zhang and G. Asplund, "Active DC filter for HVDC systems," *IEEE Comput. Appl. Power*, vol. 7, no. 1, pp. 40–44, Jan. 1994.

[11] A. Li, Z. Cai, Q. Sun, X. Li, D. Ren, and Z. Yang, "Study on the dynamic performance characteristics of HVDC control and protections for the HVDC line fault," in *Proc. IEEE Power Energy Soc. General Meeting*, Jul. 2009, pp. 1–5.

[12] J. Lenz and A. S. Edelstein, "Magnetic sensors and their applications," *IEEE Sensors J.*, vol. 6, no. 3, pp. 631–649, Jun. 2006.

[13] S. Ziegler, R. C. Woodward, H. H.-C. Iu, and L. J. Borle, "Current sensing techniques: A review," *IEEE Sensors J.*, vol. 9, no. 4, pp. 354–376, Apr. 2009.

[14] P. Ripka and M. Janosek, "Advances in magnetic field sensors," *IEEE Sensors J.*, vol. 10, no. 6, pp. 1108–1116, Jun. 2010.

[15] K. Zhu, W. K. Lee, and P. W. T. Pong, "Non-contact electric-coupling-based and magnetic-field-sensing-assisted technique for monitoring voltage of overhead power transmission lines," in *Proc. IEEE Sensors Conf.*, Nov. 2015, pp. 1–4.

[16] K. Zhu, W. K. Lee, and P. W. T. Pong, "Non-contact capacitive-coupling-based and magnetic-field-sensing-assisted technique for monitoring voltage of overhead power transmission lines," *IEEE Sensors J.*, vol. 17, no. 4, pp. 1069–1083, Feb. 2017.

[17] M. Zimmermann and K. Dostert, "An analysis of the broadband noise scenario in powerline networks," in *Proc. Int. Symp. Powerline Commun. Appl.*, 2000, pp. 131–138.

[18] Z. Tao, Y. Xiaoxian, Z. Baohui, N. H. Xu, F. Xiaoqun, and L. Changxin, "Statistical analysis and modeling of noise on 10-kV medium-voltage power lines," *IEEE Trans. Power Del.*, vol. 22, no. 3, pp. 1433–1439, Jul. 2007.

[19] M. Saint-Laurent and M. Swaminathan, "Impact of power-supply noise on timing in high-frequency microprocessors," *IEEE Trans. Adv. Packag.*, vol. 27, no. 1, pp. 135–144, Feb. 2004.

[20] D. A. Douglass, "Potential transformer accuracy at 60Hz voltages above and below rating and at frequencies above 60 Hz," *IEEE Trans. Power App. Syst.*, vol. PAS-100, no. 3, pp. 1370–1375, Mar. 1981.

[21] (2009). *Hall Effect Voltage Sensor*. J&D Electronics. Accessed: Jan. 9, 2019. [Online]. Available: https://ehqsensing.en.ec21.com/Hall_Effect_Voltage_Sensor–3491072_3491761.html

[22] B. Lee, "Review of the present status of optical fiber sensors," *Opt. Fiber Technol.*, vol. 9, no. 2, pp. 57–79, 2003.

[23] T. Mitsui, K. Hosoe, H. Usami, and S. Miyamoto, "Development of fiber-optic voltage sensors and magnetic-field sensors," *IEEE Trans. Power Del.*, vol. PWRD-2, no. 1, pp. 87–93, Jan. 1987.

[24] K. Kyuma, S. Tai, M. Nunoshita, N. Mikami, and Y. Ida, "Fiber-optic current and voltage sensors using a $Bi_{12}GeO_{20}$ single crystal," *J. Lightw. Technol.*, vol. 1, pp. 93–97, Mar. 1983.

[25] G. Wild and S. Hinckley, "Acousto-ultrasonic optical fiber sensors: Overview and state-of-the-art," *IEEE Sensors J.*, vol. 8, no. 7, pp. 1184–1193, Jul. 2008.

[26] (2017). *Non-Contact AC Voltage Probe SP3000*. HIOKI. Accessed: Jan. 8, 2019. [Online]. Available: https://www.hioki.com/en/products/detail/?product_key=6409

[27] D. Lawrence, J. S. Donnal, S. Leeb, and Y. He, "Non-contact measurement of line voltage," *IEEE Sensors J.*, vol. 16, no. 24, pp. 8990–8997, Dec. 2016.

[28] F. D. Surianu, "Determination of the induced voltages by 220 kV electric overhead power lines working in parallel and narrow routes. Measurements on the ground and mathematical model," *WSEAS Trans. Power Syst.*, vol. 4, no. 8, pp. 264–274, 2009.

[29] K. Zhu and P. W. T. Pong, "Fault classification of power distribution cables by detecting decaying DC components in fault currents with magnetic sensing," in *Proc. IEEE Int. Instrum. Meas. Technol. Conf.*, May 2018, pp. 2175–2177.

[30] C. K. C. Arruda and A. C. S. Lima, "Corona modeling in HVDC transmission lines based on a modified particle-in-cell approach," *Electr. Power Syst. Res.*, vol. 125, pp. 91–99, Aug. 2015.

[31] Y. Jiang, N. Zheng, G. Guo, R. Zhang, and X. Fu, "Corona discharge and electromagnetic environment degradation of aging transmission lines," *Int. J. Plasma Environ. Sci. Technol.*, vol. 9, pp. 35–39, Jan. 2015.

[32] J. Liu, J. Zou, J. Tian, and J. Yuan, "Analysis of electric field, ion flow density, and corona loss of same-tower double-circuit HVDC lines using improved FEM," *IEEE Trans. Power Del.*, vol. 24, no. 1, pp. 482–483, Jan. 2009.

[33] A. J. Otto and H. C. Reader, "HVDC corona space charge modeling and measurement," *IEEE Trans. Power Del.*, vol. 26, no. 4, pp. 2630–2637, Oct. 2011.

[34] F. Xiao, B. Zhang, J. Mo, and J. He, "Calculation of 3-D ion-flow field at the crossing of HVdc transmission lines by method of characteristics," *IEEE Trans. Power Del.*, vol. 33, no. 4, pp. 1611–1619, Aug. 2018.

[35] Z.-P. Zhang, G.-Z. Zhang, X. Wu, B.-Q. Wan, and Y. Lu, "Research on electromagnetic environmental parameters control indexes of ± 800 kV UHV DC transmission lines," *Power Syst. Clean Energy*, vol. 24, pp. 1–15, Apr. 2008.

[36] Y. Zhen *et al.*, "Ion flow field analysis considering the finite conductivity of the building near HVDC transmission lines," *IEEE Trans. Magn.*, vol. 51, no. 3, Mar. 2015, Art. no. 7202704.
[37] (2014). *What are the Ways to Reduce Corona Loss in Transmission Lines?* Quora. [Online]. Available: Accessed: Nov. 14, 2018. https://www.quora.com/What-are-the-ways-to-reduce-corona-loss-in-transmission-lines
[38] U. Corbellini and P. Pelacchi, "Corona losses in HVDC bipolar lines," *IEEE Trans. Power Del.*, vol. 11, no. 3, pp. 1475–1481, Jul. 1996.
[39] Y. Zhen *et al.*, "Calculating charged electric potential of the conductor in ionized field," in *Proc. Chin. Soc. Elect. Eng.*, vol. 31, no. 27, pp. 8–13, 2011.
[40] (2016). *Why is the Earth at Zero Potential?* Quora. Accessed: Nov. 15, 2018. [Online]. Available: https://www.quora.com/Why-is-the-earth-at-zero-potential
[41] F. Dawalibi, "Ground fault current distribution between soil and neutral conductors," *IEEE Trans. Power App. Syst.*, vol. PAS-99, no. 2, pp. 452–461, Mar. 1980.
[42] F. Dawalibi and G. B. Niles, "Measurements and computations of fault current distribution on overhead transmission lines," *IEEE Trans. Power App. Syst.*, vol. PAS-103, no. 3, pp. 553–560, Mar. 1984.
[43] (2017). *VSC-Based HVDC Transmission System*. MathWorks. Accessed: Apr. 19, 2017. [Online]. Available: http://ow.ly/pLlK30aYcOE
[44] (2015). *Introduction to TMR Magnetic Sensors*. Multidimensions. Accessed: Nov. 6, 2018. [Online]. Available: http://www.dowaytech.com/en/1776.html
[45] K. Zhu, W. Han, W. K. Lee, and P. W. T. Pong, "On-site non-invasive current monitoring of multi-core underground power cables with a magnetic-field sensing platform at a substation," *IEEE Sensors J.*, vol. 17, no. 6, pp. 1837–1848, Mar. 2017.
[46] P. P. Freitas, R. Ferreira, S. Cardoso, and F. Cardoso, "Magnetoresistive sensors," *J. Phys., Condens. Matter*, vol. 19, no. 16, p. 165221, 2007.
[47] (2011). *3-axis Magnetic Sensor Hybrid HMC2003*. Honeywell. Accessed: Dec. 11, 2017. [Online]. Available: https://neurophysics.ucsd.edu/Manuals/Honeywell/HMC_2003.pdf
[48] K. Zhu and P. W. T. Pong, "Performance study on commercial magnetic sensors for measuring current of unmanned aerial vehicles," in *Proc. IEEE Int. Instrum. Meas. Technol. Conf.*, May 2018, pp. 1–3.
[49] K. Zhu, W. K. Lee, and P. W. T. Pong, "Energization-status identification of three-phase three-core shielded distribution power cables based on non-destructive magnetic field sensing," *IEEE Sensors J.*, vol. 17, no. 22, pp. 7405–7417, Nov. 2017.
[50] R. Kiranmayi. (2013). *Reduction of Harmonics in HVDC Transmission System using High Pulse Converter*. Accessed: Dec. 4, 2017. [Online]. Available: https://www.ijircce.com/upload/2013/june/39_paper12.pdf
[51] G. N. Bathurst, B. C. Smith, N. R. Watson, and J. Arrillaga, "Modelling of HVDC transmission systems in the harmonic domain," *IEEE Trans. Power Del.*, vol. 14, no. 3, pp. 1075–1080, Jul. 1999.
[52] A. D'Amico and C. Di Natale, "A contribution on some basic definitions of sensors properties," *IEEE Sensors J.*, vol. 1, no. 3, pp. 183–190, Oct. 2001.
[53] D. Middleton, "Statistical-physical models of electromagnetic interference," *IEEE Trans. Electromagn. Compat.*, vol. EMC-19, no. 3, pp. 106–127, Aug. 1977.
[54] (2017). *Signal Processing: Smoothing*. OriginLab. Accessed: Dec. 4, 2017. [Online]. Available: https://www.originlab.com/doc/Origin-Help/Smoothing
[55] X. Liu *et al.*. (2016). "Overview of spintronic sensors, Internet of Things, and smart living." Accessed: Jan. 17, 2019. [Online]. Available: https://arxiv.org/abs/1611.00317
[56] H. Farhangi, "The path of the smart grid," *IEEE Power Energy Mag.*, vol. 8, no. 1, pp. 18–28, Jan./Feb. 2010.

Ke Zhu was born in Yichang, China, in 1990. He received the B.Eng. degree in electrical engineering from China Three Gorges University, China, in 2013, and the Ph.D. degree in electrical and electronic engineering from The University of Hong Kong in 2018. He is currently a Post-Doctoral Researcher with The University of Hong Kong. His current research and academic interests focus on computational electromagnetics, electric power transmission monitoring, and application of magnetoresistive sensors in smart grid.

Wing Kin Lee received the B.Sc. and M.Sc. degrees from The University of Hong Kong, in 1976 and 1988, respectively, and the M.B.A. degree from The Chinese University of Hong Kong in 1990. He is a professional in electrical services and power engineering, and is currently a Senior Teaching Consultant with The University of Hong Kong. He has earned industrial experience while involved with power and communication utility companies in Hong Kong. His current research interests include smart grid demand side management, electrical load signature, and vertical transportation.

Philip W. T. Pong received the B.Eng. (Hons.) degree in electrical and electronic engineering from The University of Hong Kong (HKU) in 2002, and the Ph.D. degree in engineering from the University of Cambridge in 2005.

After working as a Post-Doctoral Researcher at the Magnetic Materials Group, National Institute of Standards and Technology, Gaithersburg, MD, USA, for three years, he joined the HKU Department of Electrical and Electronic Engineering, in 2008, where he is currently an Associate Professor, working on the development of magnetoresistive sensors, and the applications of MR sensors in smart grid and smart living. He is serving on the Administrative Committee of the IEEE Magnetics Society.

Dr. Pong is a Fellow of the Institute of Materials, Minerals and Mining, a Fellow of the NANOSMAT Society, and a Corporate Member of Hong Kong Institution of Engineers (HKIE) in Electrical Division, Electronics Division and Energy Division. He serves as an Editorial Board Member for three SCI journals. He was a recipient of the HKIE Young Engineer of the Year Award in 2016. He is also a Chartered Physicist, Chartered Energy Engineer, and a Registered Professional Engineer.